Contents

Chapter 1

Theory

Contents

1.1 Sesquioxides

Transparent Conductive Oxides (TCOs) are materials that combine the properties of having low absorption coefficient in the visible spectrum and being conductive at the same time [1]. The interest in these materials is motivated by possible applications in portable and flexible electronics [2], displays [3], solar cells [4] and more [1]. Not only the focus on a small number of materials in the past (SnO_2, In_2O_3, ZnO) [1], but also the scarcity and concerns about availability[(1)] of fundamental compounds [5] increases the demand for new materials. This includes fabrication of *p*-type TCOs as well as compounds with even larger band gaps than 3 eV, called Ultrawide-bandgap (UWBG) materials. Because the critical electrical field – at which breakdown occurs – is depending on the band gap [6], UWBG materials can serve for high-power electronic devices as well as for deep ultra-violet (UV) optoelectronics [7]. Candidates for this material class are group-III sesquioxides[(2)], of which Ga_2O_3 with its several polymorphs

(1) China controls 75 % of the world's indium reserves, and limited the export of this material already in the past [5].

(2) A sesquioxide is an oxide with formula unit Me_2O_3, where Me is a metal with oxidation state +3. Transition metal sesquioxides are, e.g., Y_2O_3, Rh_2O_3 or In_2O_3.

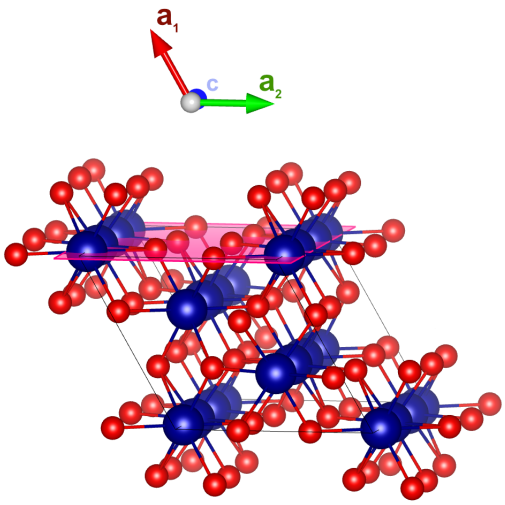

Figure 1.1: Image of the rhombohedral Cr_2O_3 crystal structure. Blue and red spheres correspond to Cr and O atoms, respectively. The magenta plane is the (10.0) *m*-plane. The image was made using VESTA Ver. 3 [**momma2011**].

[8] recently gained interest in the scientific community – in particular the metastable corundum structured α-Ga_2O_3.

The sesquioxide Cr_2O_3, being a possible *p*-type TCO, is isomorphic to group-III sesquioxide α-Ga_2O_3 with quite similar lattice parameters (cf. Tab. 1.1). This enables the use of Cr_2O_3 as a buffer layer between α-Ga_2O_3 and isomorphic α-Al_2O_3 (sapphire) substrates to improve the crystal quality [9]. The lower band gap also makes band gap engineering with isostructural sesquioxides interesting [10] and finally, Cr_2O_3 exhibits increased conductivity upon doping [11] and could thus serve as *p*-type component in a *p*-*n*-heterojunction with α-Ga_2O_3. In the following, an overview of the two mentioned sesquioxides will be presented with focus on the physical properties being relevant to this work.

1.1.1 Chromium Oxide

Chromia or *Eskolaite* is a sesquioxide composed of the transition metal chromium and oxygen with formula unit Cr_2O_3. Other chromium oxides do exist (e.g. metallic CrO_2, toxic CrO_3), but Cr_2O_3 is the thermodynamically most stable oxidation state [12–14], making it the abundant chromium oxide on earth [15].

Chromium oxide is used for a wide range of applications, in particular it can be utilized as a coating material due to its high hardness [17], sufficient transparency for low thicknesses [18] as well as its resistance against corrosion and oxidation [19]. This also explains its use-case as component of stainless steel to form passive films [14]. Cr_2O_3 thin films absorb electromagnetic waves with wavelengths smaller than 400 nm, making it opaque in the UV-spectrum [20, 21]. It is transparent in the visible spectrum with, e.g., a reported transmittance of 40 % at 700 nm for 0.5 µm thick films by Cheng *et al.* (1996) [20].

Cr_2O_3 crystallizes in the corundum structure, which has trigonal symmetry (space

Table 1.1: Lattice constants of selected corundum structured sesquioxides.

	a	c	Ref.
α-Al_2O_3	4.76 Å	13.00 Å	Pishchik *et al.* (2009) [26]
α-Cr_2O_3	4.96 Å	13.59 Å	Mi *et al.* (2018) [15]
α-Ga_2O_3	4.98 Å	13.43 Å	Marezio and Remeika (1967) [27]

Table 1.2: Several deposition techniques that have been applied on Cr_2O_3.

Deposition technique	Substrate	Reference
Chemical Vapor Deposition (CVD)	Si(111)	[28, 29]
	glass	[20]
Molecular Beam Epitaxy (MBE)	c-sapphire	[23, 30]
Thermal evaporation	Pt(111)	[12]
Electron-beam Physical Vapor Deposition (PVD)	glass	[13]
Spray pyrolysis	glass	[31]
radio-frequency (RF) sputtering	c-sapphire	[9, 32]
	r-sapphire	[33]
Reactive direct current (DC) sputtering	glass	[21]
Reactive Pulsed Laser Deposition (PLD)	Si(100)	[34]
	r-sapphire	[35]
Non-reactive PLD	c-sapphire	[23, 36, 37]

group $R\bar{3}c$) and belongs to the hexagonal crystal family. One unit cell contains six formula units, i.e. 12 chromium cations and 18 oxygen anions [14]. The oxygen atoms arrange in a hexagonal close-packed manner, where two thirds of the formed octahedrons are filled with Cr atoms [22]. The unit cell is spanned by a principal axis, called c-axis[(3)], with lattice constant c, and a hexagonal basal plane with lattice constant a. The numerical values for those lattice parameters differ depending on the publication [9, 15, 23–25], and henceforth the values in Tab. 1.1 will be used [15, 26, 27]. Only one study is known to the author that states another cubic spinel γ-phase with random missing Cr point defects [12]. This information is based on Wyckoff (1963) [16], but the source is not available, so no further information can be given about the stability or other properties of this potential phase. Henceforth, Cr_2O_3 will refer to the α-phase.

Several techniques combined with various substrates were applied for depositing chromia thin films, which are listed in Tab. 1.2. The first deposition via PLD was done by Tabbal *et al.* (2006) [38].

Electronic Structure Experimental and theoretical studies reveal that chromia exhibits a band gap of 3.2 to 3.4 eV [12, 14, 15, 25] making it a wide band gap material. Discussion on the p-type or insulating behavior of Cr_2O_3 can be found in literature: With only a few defects, high quality epitaxial films of Cr_2O_3 grown by MBE [30] or PLD [23] are not p-type. This insulating behavior is classified as both Mott-Hubbard

(3) The spins of the Cr atoms along this direction are alternating 3 ↑ and 3 ↓ [23], making the crystal antiferromagnetic [14, 22].

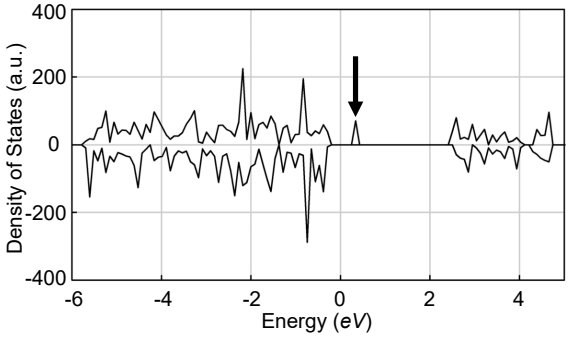

Figure 1.2: Calculated density of states (DOS) of chromia, taking a V_{Cr} into account. The arrow marks the new acceptor level. Reprinted with permission from Lebreau *et al.* (2014) [14]. Copyright © 2014 American Chemical Society.

type and charge-transfer type, which are models to describe the electronic behavior of compounds containing transition metals with partly filled $3d^n$ orbitals, with $n = 5$ for Cr [14, 15, 22]. Density Functional Theory (DFT) calculations show that the Cr-3d states are almost solely responsible for electronic states in the conduction band and that they are also present in the valence band [14, 15]. Thus, $3d \longrightarrow 3d$ band transitions are possible, indicating that the Mott-Hubbard model might fit best for this compound [14]. However, the O-2p states are mainly present in the valence band at similar energies as the Cr-3d states, which leads to hybridization and thus indicating the charge-transfer model [14].

However, several studies agree on Cr_2O_3 being a semiconductor with p-type conductivity at room temperature and atmospheric conditions [14, 15, 20, 32, 34, 36, 40]. Calculations were performed to investigate the effect of point defects on the band structure and conductivity. When considering a missing chromium atom (*vacancy* V_{Cr}), the band structure changes in two ways: The band gap itself is reduced [15], but not sufficiently to make excitations of valence electrons into the conduction band more probable than for defectless chromia. Additionally, there is a new defect band introduced slightly above the Fermi level (cf. Fig. 1.2), which acts as an unoccupied acceptor level [15]. This defect state is mainly composed of O-2p orbitals of the oxygen anions surrounding the vacancy [14]. Effectively, a missing neutral chromium atom removes the Cr^{3+} cation as well as three electrons bound to the adjacent O^{2-} anions, thus creating three holes [14] explaining the p-type conductivity.

Note that there are also other possible defects with different effects: a chromium Frenkel point defect describes a Cr atom leaving it's position and occupying a formerly unoccupied cavity in one of the oxygen-octahedrons. This Frenkel defect creates a new band below the Fermi level, acting as an occupied donor level [14]. A similar defect state is introduced by oxygen vacancies [15]. Note that the Fermi level is located only slightly above the Valence Band Maximum (VBM) and thus the new occupied donor level is not significantly closer to the Conduction Band Minimum (CBM), which means that electrons still have to overcome the band gap energy to get into conducting states. This favors the formation of holes via Cr vacancies (O-2p acceptor states) rather than electrons via Cr Frenkel defects and O vacancies (Cr-3d donor states).

Doping Several attempts have been made to alter the conductivity of chromia thin films deliberately, including incorporation of magnesium [11, 30, 31], nickel [37], or lithium [41, 42] to achieve better *p*-type conductivity On the other hand, incorporation of titanium yields electrons as majority carriers [43] due to the higher valent state of Ti when substituting Cr sites (Ti_{Cr}) [40].

Especially the effect of Mg doping of Cr_2O_3 thin films has been reported in literature. [11, 23, 25, 30, 31, 37, 43]. Substituting Cr atoms with less valent hole providers – compared to structural defects of pure Cr_2O_3 – does not only allow for a more controlled defect incorporation, but is also energetically more favorable due to a lower formation energy of Mg_{Cr} compared to V_{Cr} [23]. Uekawa and Kaneko (1996) [11] report an increase in conductivity of five orders of magnitude for Cr_2O_3:Mg thin films prepared by the polymer precursor method. This result can be further improved by postannealing [30] and deposition at higher oxygen partial pressures [30, 43]. These effects are attributed to homogenization of magnesium inside the thin films and increased MgO incorporation during deposition, respectively. An observed side-effect of Mg-doping is a color change to a brownish tint [11, 25]. Uekawa and Kaneko (1996) [11] discuss that this may be the result of a mixed valence state of chromium (Cr^{4+} or Cr^{6+}), formed upon doping, as observed by X-ray Photoelectron Spectroscopy (XPS). This may establish an unoccupied state, favoring charge-transfer transitions from O-2*p* orbitals to this low-energetic state, resulting in a different optical appearance of the thin films. However, it has been shown that the overall transparency can be increased by codoping of Mg with nitrogen which also reduces the decolorization substantially [25, 31].

1.1.2 Gallium Oxide

Ga_2O_3 is a group-III sesquioxide with four[(4)] different polymorphs, of which β-Ga_2O_3 is the thermodynamically most stable one at ambient conditions [8, 44, 45]. The corundum-structured α-Ga_2O_3 phase, which is of most relevance for this work, is isomorphic to Cr_2O_3, with lattice parameters as listed in Tab. 1.1. Note that Cr_2O_3 has a larger *c* lattice constant, but a smaller *a* lattice constant than α-Ga_2O_3. However, both compounds have larger lattice constants than Al_2O_3. α-Ga_2O_3 is thermodynamically metastable [46], i.e. the phase can exist under ambient conditions, even though β-Ga_2O_3 has a lower energy state up to 1800 °C [47]. The thermodynamic equilibrium – which determines the favored phase – can also be changed by strain due to lattice mismatch occurring during heteroepitaxy. [45]. This approach is of particular interest due to the possibility of deposition on cheap – compared to bulk β-Ga_2O_3 substrates [46, 48] – and readily available sapphire substrates which are isomorphic to α-Ga_2O_3 [33, 46, 47]. Note that deposition of β-Ga_2O_3 on sapphire is also possible, but only with restriction to formation of more than one crystal domain [48]. On the other hand, highly crystalline [47] α-Ga_2O_3 thin films can be grown without rotational domains [45, 48].

Deposition of α-Ga_2O_3 on sapphire has been done by several deposition techniques, including [48]: Halide Vapor Phase Epitaxy (HVPE), mist CVD [49], MBE [44], Atomic Layer Deposition and metalorganic CVD. Phase-pure deposition via PLD has also been achieved [44, 45, 50]. Despite being isomorphic to each other, α-Ga_2O_3 and sapphire

(4) Five, if the δ-phase is not considered as a form of the ϰ-phase [8].

still exhibit a lattice mismatch of around 4.8 % along the a-axis [46]. This induces semicoherent growth with a fairly high dislocation density, which has been reported to be around $7 \times 10^{10}\,\mathrm{cm}^{-2}$ [49]. In particular, this becomes a problem regarding carrier mobility which is tremendously hindered by dislocation scattering [46].

To overcome the problems of lattice mismatch between sapphire substrates and α-Ga_2O_3 thin films, quasi-continuous gradients from Al_2O_3 to α-Ga_2O_3 have been applied, utilizing the capability of alloying the respective compounds [51]. Furthermore, buffer layers of isomorphic Cr_2O_3 have been used to decrease the high dislocation density for deposition on c-oriented [9, 32] as well as r-oriented sapphire [33]. Deposition on other than c-oriented substrates also decreases parasitic phases because of the suppression of c-plane facets on m- and a-plane sapphire [52]. Deposition on prismatic m-plane sapphire also yields much higher carrier mobilities when compared to c-plane sapphire [53]. It has to be noted that despite the difficulties occurring upon lattice mismatch, pseudomorphic growth seems to be feasible without buffer layers for different deposition techniques, at least for some monolayers [44].

With 5.0 to 5.3 eV [48], α-Ga_2O_3 has the highest band gap of the four polymorphs [47]. Band gap engineering is possible by alloying with Al_2O_3 [52] or In_2O_3 [54]. The crystal structure also allows for alloying with other corundum structured compounds [48], in particular other transition metal oxides such as Cr_2O_3 [32, 33]. The conduction band is mainly composed of Ga-4s states with an effective electron mass of $0.3\,m_e$. The valence band is very flat and mainly composed of O-2p orbitals, yielding a high effective electron mass and thus strong localization [47]. This hinders the realization of p-type α-Ga_2O_3. Next to band gap engineering, n-type doping via Sn, Si and Ge [50], as well as Zr [55] incorporation has been accomplished.

1.2 X-ray Diffraction Principles

1.2.1 Scattering at Lattices

To elucidate the working principles behind X-ray diffraction (XRD) as a measurement method (cf. 2.2), a brief description of reciprocal space and constructive interference will be provided. Those derivations are based on Ashcroft and Mermin (1976) [56].

A periodic point-like structure with translational symmetry ("Bravais lattice") can be described by three vectors $\mathbf{a}_i$ that span a so-called "unit cell". Every lattice point $\mathbf{R}$ is a linear combination of those unit cell vectors. For such a lattice, there exists a so-called "reciprocal lattice", which consists of all vectors $\mathbf{K}$ satisfying the condition[5]:

$$e^{i\langle \mathbf{K},\mathbf{R}\rangle} = 1\,, \tag{1.1}$$

$$\Leftrightarrow \langle \mathbf{K},\mathbf{R}\rangle = 2\pi m\,, \tag{1.2}$$

with $m \in \mathbb{N}$. This is again a Bravais lattice with unit cell vectors $\mathbf{a}_j^*$:

$$\mathbf{K}_{hkl} = h\mathbf{a}_1^* + k\mathbf{a}_2^* + l\mathbf{a}_3^*\,. \tag{1.3}$$

It follows that for any i, j:

$$\langle \mathbf{a}_i^*, \mathbf{a}_j\rangle = 2\pi\delta_{ij}\,, \tag{1.4}$$

[5] The definition of $\mathbf{K}$ by (1.1) is a consequence of demanding that the plane wave described by $f_{\mathbf{K}}(\mathbf{r}) = \exp(i\langle \mathbf{K},\mathbf{r}\rangle)$ has the same symmetry as the Bravais lattice [56].

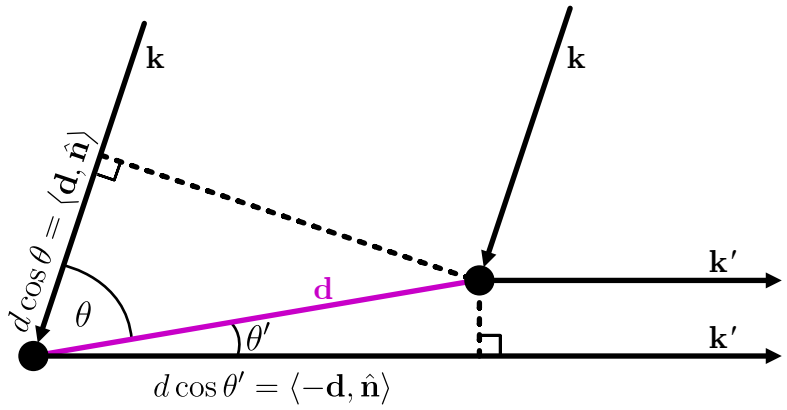

Figure 1.3: The geometry of two scattering centers displaced by $\mathbf{d}$, as well as incident and reflected X-rays $\mathbf{k}$ and $\mathbf{k}'$, respectively.

with the KRONECKER delta δ_{ij}. A major application of reciprocal space vectors is their ability to describe lattice planes. Any lattice plane can be described by the shortest possible reciprocal space vector $\mathbf{K}_{hkl}$ perpendicular to it. Consequently, the lattice plane is denoted by (hkl). The distance between equivalent lattice planes can be calculated via

$$d_{hkl} = |\mathbf{K}_{hkl}|^{-1} \,. \tag{1.5}$$

Note that for non-cubic crystals, the lattice plane (hkl) is in general *not* perpendicular to the lattice direction [hkl].

With those preliminarities, the conditions for constructive interference during diffraction of radiation at BRAVAIS lattices can be derived. Consider two scattering centers separated by $\mathbf{d}$ (Fig. 1.3) and incident radiation with wave vector $\mathbf{k}$:

$$\mathbf{k} = \frac{2\pi}{\lambda}\hat{\mathbf{n}} \,, \tag{1.6}$$

with wavelength λ and direction $\hat{\mathbf{n}}$. For the case of elastic scattering, the outcoming wave vector $\mathbf{k}'$ has the same wavelength λ but different direction $\hat{\mathbf{n}}'$. The phase difference of two photons scattered at the 1st and 2nd scattering center, respectively, can be calculated from their path difference, which reads

$$\langle \mathbf{d}, \hat{\mathbf{n}} \rangle + \langle -\mathbf{d}, \hat{\mathbf{n}}' \rangle \,. \tag{1.7}$$

Constructive interference occurs, if the phase difference is an integral multiple of the wavelength, so it must follow that

$$\langle \mathbf{d}, (\hat{\mathbf{n}} - \hat{\mathbf{n}}') \rangle = m\lambda \tag{1.8}$$

$$\Leftrightarrow \langle \mathbf{d}, (\hat{\mathbf{k}} - \hat{\mathbf{k}}') \rangle = 2\pi m \,, \tag{1.9}$$

with $m \in \mathbb{N}$. Comparing with Equ. (1.2) reveals that $\hat{\mathbf{k}} - \hat{\mathbf{k}}'$ is a reciprocal space vector, because the separation $\mathbf{d}$ of the two scattering centers is a lattice vector $\mathbf{R}$. So constructive interference (observing a reflection) occurs if and only if the scattering geometry (determined by angle of incidence and refraction, as well as wavelength) matches the

lattice symmetry in the sense that there is a corresponding lattice translation vector $\mathbf{d}$ fulfilling Equ. (1.9). Thus, from the position of reflections in reciprocal space, one can deduce the lattice symmetry.

Note that this description of X-ray scattering is equivalent to the Bragg condition:

$$m\lambda = 2d_{hkl}\sin(\theta)\,, \tag{1.10}$$

where the angle of incidence θ and λ are contained in $\hat{\mathbf{k}} - \hat{\mathbf{k}}'$. Furthermore, when a lattice point is not equivalent to a single atom, but represents several scattering centers, an additional geometrical structure factor has to be taken into account to determine whether a certain geometry allows reflexes. This is important, e.g., for structures with trigonal symmetry. They are described with a conventional hexagonal unit cell, although not every plane (hkl) exhibits constructive interference. The condition for allowed reflections is $-h + k + l = 3n$, with $n \in \mathbb{N}_0$ [57].

1.2.2 X-rays

Atomic distances in solids are of the order of several Å, so the radiation for probing those structures must have a similarly sized wavelength, which is fulfilled by X-rays [58]. The following description of X-rays is based on Spieß (2009) [59].

The basis of any X-ray tube are high-energy electrons which are produced by thermionic emission in a cathode, which is usally made out of tungsten[(6)]. An electric field of several kV accelerates the electrons to the anode, where they are stopped such that around 99 % of their kinetic energy dissipates. The momentum change of electrons, which are charged particles, leads to emission of bremsstrahlung. Furthermore, the electrons ionize atoms of the anode material which leads to unoccupied electron states. If those states are filled by electrons with higher quantum number n, the difference in energy of those levels is emitted as radiation with a discrete spectrum, called characteristic X-ray. Important for XRD measurements is a part of the characteristic spectrum, called K-radiation, which originates in occupation of empty $1s$-orbitals. The occupying electron must come from an orbital with angular momentum quantum number $l = 1$, i.e. a p-orbital, because Δl cannot be zero for intraatomic electron transitions. The radiation is termed Kα- or Kβ-radiation, depending on whether the previous orbital was $2p$ or $3p$, respectively. Furthermore, one distinguishes $K\alpha_1$- and $K\alpha_2$-radiation, depending on the magnetic quantum number of the previous orbital, which can be $\frac{3}{2}$ or $\frac{1}{2}$, respectively. Kα-radiation is desired for probing crystal structures.

1.3 Heteroepitaxy

1.3.1 Pseudomorphic Growth

When a body is deformed (*strained*) from its original state of equilibrium (*bulk*), forces will arise that tend to return the body to this equilibrium. Molecular forces are the driving element behind these stresses [60]. In continuum mechanics, stress σ_{ij} and

(6) Tungsten is the element with the second highest melting point of around 3400 °C. This ensures a low contamination of the anode with cathode material, reducing the intensity of observed peaks in XRD patterns that correspond to tungsten (cf. 2.2).

Table 1.3: The six independent entries of the elasticity tensor for rhombohedral Cr_2O_3 [62] and α-Ga_2O_3 [61]. All values are in units of 100 GPa.

Material	C_{11}	C_{12}	C_{13}	C_{33}	C_{44}	C_{14}
α-Cr_2O_3	3.74	1.48	1.75	3.62	1.59	−0.19
α-Ga_2O_3	3.82	1.74	1.26	3.46	0.78	−0.17

strain ϵ_{kl} are symmetric rank-2 tensors that are linearly connected by the elasticity tensor with components C_{ijkl}:

$$\sigma_{ij} = \sum_{k,l} C_{ijkl}\epsilon_{kl} \,. \tag{1.11}$$

Note that Equ. (1.11) represents a set of 9 linear equations.

If the in-plane (i.p.) lattice constants of two isomorphic compounds match at the interface of a heterostructure, one refers to "pseudomorphic" growth. This confines a part of the system of equations (1.11):

1. The thin film i.p. lattice constants $a_{\parallel}^{F}$ have to match the substrate i.p. lattice constants $a_{\parallel}^{S}$. This defines the magnitude of i.p. strain of the thin film material.

2. On the other hand, due to vertical growth, the out-of-plane (o.o.p.) stress of the thin film is demanded to be zero: $\sigma_{zz} = 0$.

The resulting o.o.p. strain as well as non-diagonal strain components can be derived by solving the system of equations (1.11) with these two boundary conditions. In Grundmann (2018) [61], formulas are derived for the unknown strains in the special case of pseudomorphic heterostructures with threefold rhombohedral symmetry. For quantitative predictions of those strains, the elasticity tensor C_{ijkl} of the thin film compound has to be known. Depending on the symmetry of the crystal structure, its components collapse into a lower number of independent entries. Due to symmetry reasons [56], the nine indices ij of the strain tensor can be unambiguously expressed by one index with six possible values: $11 \to 1$, $22 \to 2$, $33 \to 3$, $23 \to 4$, $13 \to 5$, $12 \to 6$ [61]. This allows for a 6×6-matrix representation of the elasticity tensor $C_{ijkl} \to C_{\mu\nu}$. For rhombohedral crystals, six independent components are left [56]. The entries of the elasticity tensor of the two sesquioxides important for this work are given in Tab. 1.3.

Because of its direct influence on the o.o.p. lattice plane distance and thus on the XRD patterns of 2θ-ω-scans (cf. 2.2), the strain component perpendicular to the sample surface, ϵ_{zz}, is of particular interest. In the following, the formulas for the case of rhombohedral crystal structures are stated as derived in Grundmann (2018) [61]. They depend on the respective i.p. strains ϵ_{xx} and ϵ_{yy} caused by the lattice mismatch between film and substrate. Note that here, $\mathbf{r} = (x, y, z)$ describes coordinates in the laboratory system – in contrary to Ref. [61], where $\mathbf{r}$ and $\mathbf{r}'$ are used to describe cartesian coordinates in the crystal and laboratory system, respectively.

One derives for (11.0)-plane (a-orientation):

$$\epsilon_{zz,a} = -\frac{C_{13}\epsilon_{xx,a} + C_{12}\epsilon_{yy,a}}{C_{11}} \,, \tag{1.12}$$

Table 1.4: **(a)** Comparison of d and d_{str}, which are the o.o.p. lattice plane distances for bulk Cr_2O_3 and pseudomorphic Cr_2O_3 on Al_2O_3, respectively. The corresponding o.o.p.-strain ϵ_{zz} is also given, as well as the corresponding angles of typical reflections in diffraction patterns of 2θ-ω-scans. **(b)** The resulting tilt of the thin film depending on substrate orientation for relaxed growth. The results are obtained from considerations on the possible slip systems and BURGER's vectors.

Orientation	**(a)** Pseudomorphic					**(b)** Relaxed	
(X-ray reflection)	d (nm)	d_{str}(nm)	ϵ_{zz}(%)	2θ (°)	$2\theta_{\mathrm{str}}$ (°)	$\theta_{T,x}$	$\theta_{T,y}$
c (00.6)	13.59	14.12	3.90	39.75	38.20	–	–
a (11.0)	2.48	2.57	3.63	36.18	34.87	no	no
m (30.0)	4.30	4.45	3.67	65.06	62.49	yes	no
r (02.4)	3.63	3.72	2.41	50.19	48.93	yes	no

for (10.0)-plane (m-orientation):

$$\epsilon_{zz,m} = -\frac{C_{13}C_{44}\epsilon_{xx,m} + (C_{12}C_{44} + C_{14}^2)\epsilon_{yy,m}}{C_{11}C_{44} - C_{14}^2}\,, \tag{1.13}$$

and for (00.1)-plane (c-orientation):

$$\epsilon_{zz,c} = -\frac{2C_{13}}{C_{33}}\epsilon_{yy,c}\,, \tag{1.14}$$

with $\epsilon_{xx,a} = c_S/c_F - 1$ and $\epsilon_{yy,a} = a_S/a_F - 1$, depending on the lattice parameters of substrate (a_S, c_S) and film (a_F, c_F). Note that

$$\begin{aligned}\epsilon_{xx,a} &= \epsilon_{xx,m}\,,\\ \epsilon_{yy,a} &= \epsilon_{yy,m}\,,\\ \epsilon_{yy,c} &= \epsilon_{yy,a}\,.\end{aligned}$$

For (01.2)-plane (r-orientation), more complex relations arise as it was demonstrated by Grundmann (2020) [63]. The distance of lattice planes d orthogonal to the sample surface are then strained, such that:

$$d_{\mathrm{strained}} = d(1 + \epsilon_{zz})\,. \tag{1.15}$$

Assuming pseudomorphic growth of Cr_2O_3 on Al_2O_3, one can compare the strained lattice plance distances to the unstrained bulk values, by utilizing (1.15). The numerical values, calculated from the lattice constants (Tab. 1.1) and the elasticity tensor (Tab. 1.3), are listed in Tab. 1.4a.

1.3.2 Relaxed Growth

Dislocations

When the lattice mismatch is not resolved by adaption to the substrate (cf. 1.3.1), the strain is relieved by formation of *dislocations*, which faciliate a relaxed growth mode

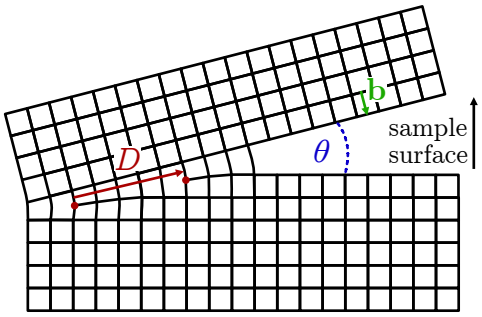

Figure 1.4: Edge dislocation with BURGER's vector perpendicular to the sample surface. The edge dislocation lines are indicated by the red dots and are perpendicular to the image plane. Consequently, the direction of the edge BURGER's vector is indicated by the red arrow, whose length D denotes the distance between dislocation lines. The green BURGER's vector **b** is the orthogonal component $b_\perp$ mentioned in the text.

of the film [64]. The highest disturbance from equilibrium spacing occurs close to the *dislocation line* which extends through the material – far away from this line, the crystallinity is restored. In which fashion the distortion happens, can be characterized by the BURGER's vector **b**. The relation of the BURGER's vector to the dislocation line determines the type of the dislocation: if they are orthogonal, one refers to an *edge* dislocation; if they are parallel, one refers to a *screw* dislocation. For a "perfect" dislocation[(7)], the BURGER's vector is a lattice translation vector. Note that in general, dislocations exhibit both edge- and screw-character [66].

Dislocations are not static, but can move ("glide") inside the crystal. The movement happens typically inside a plane which has highest density of atoms ("glide plane") and along the BURGER's vector which is responsible for the dislocation [66]. The arrangement of glide plane and direction of movement is called "slip system", e.g. for hexagonal structures, one finds $\{00.1\}/\langle 11.0\rangle$ to be one prevailing slip system [66].

For some slip systems occuring on heterostructures, the relaxation results in an additional tilt of the deposited film. This happens because a BURGER's vector **b** has more than one component: the edge component $b_\parallel$ causes strain relaxation along $b_\parallel$; but if **b** also exhibits a component $b_\perp$ orthogonal to the sample surface and the dislocation line, a tilt angle θ_T will result between substrate and relaxed film [64, 67]:

$$\theta_{T,i} = \epsilon_{ii} \frac{b_{i,\perp}}{b_{i,\parallel}} \,, \tag{1.16}$$

where i denotes the axis of strain relaxation. This is schematically depicted in Fig. 1.4. Note that Equ. (1.16) is formulated for partially relaxed systems in Kneiß *et al.* (2021) [64], but here the relaxation parameter ρ_i was omitted, therefore assuming fully relaxed thin films.

Slip Systems for Sesquioxide Heterostructures

For heteroepitaxial growth of $(Al_xGa_{1-x})_2O_3$ with low Al content on Al_2O_3, studies have been conducted on the prevailing relaxation mechanisms for r-oriented [67, 68],

(7) Also referred to as "full" dislocation [65].

as well as a- and m-oriented [64] growth directions. In the following, those results will be summarized. Note that the x-axis points along the c-axis for m- and a-oriented heterostructures, and similarly along the projection of the c-axis on the sample surface for r-oriented heterostructures.

(01.2)-plane (r-orientation) The two relevant slip systems are $\{00.1\}/\frac{1}{3}\langle 11.0\rangle$ and $\{11.0\}/\frac{1}{3}\langle 1\bar{1}.1\rangle$, which contain the "basal" and "prismatic" glide plane, respectively [67]. The former allows relaxation along the direction containing the projection of the c-axis (x-axis), whereas the latter allows relaxation perpendicular to it (y-axis). For the basal system, one can determine two possible independent BURGER's vectors $\mathbf{b}_c$ with differing screw components but otherwise same tilt and edge components $b_{c,\perp}$ and $b_{c,\parallel}$, respectively. The tilt along x-direction can then be calculated via:

$$\theta_{T,x} = \epsilon_{xx}\frac{b_{c,\perp}}{b_{c,\parallel}} = \frac{1}{\sqrt{3}}\zeta_F\epsilon_{xx}\,, \tag{1.17}$$

with $\zeta_F = c_F/a_F$. For the prismatic slip system, the possible BURGER's vectors facilitate relaxation along the y-direction via $b_{a,\parallel}$. But in contrast to the basal system, the tilt components $b_{a,\perp}$ cancel out on average, thus resulting in no net tilt along the y-direction: $\theta_{T,y} = 0$.

(10.0)-plane (m-orientation) Neither basal (00.1) nor prismatic (11.0) and (10.0) slip systems can resolve strain along the x-axis: The (00.1)-plane is perpendicular to the surface and x-direction, thus the BURGER's vector can only have components in the y-z-plane. But for strain release along x, the BURGER's vector should have non-zero component in this direction, which cannot be the case. The prismatic planes, on the other hand, are perpendicular to the surface but parallel to the x-axis. This results in a dislocation line along the x-direction. To release strain, the BURGER's vector would have x-component, which does not apply for edge dislocations. So the prevailing slip system must have (01.2)-plane (r-orientation) or (11.2)-plane (s-orientation) character, which are called "pyramidal" slip systems. Three different r-planes contribute to strain release, because there is dislocation line component along the y-axis and BURGER's vector's components along the x-axis. With Equ. (1.16) and substituting the possible BURGER's vectors one finds:

$$\theta_{T,x} = \frac{2}{3}\frac{\sqrt{3}}{\frac{20\zeta}{24+6\zeta^2}+\zeta}\left(\frac{c_S}{c_F}-1\right) \tag{1.18}$$

(11.0)-plane (a-orientation) The same argument as for the m-oriented heterestructure holds, why only pyramidal slip systems are possible. But in this case, only two r-planes contribute to strain relaxation, because the third plane is perpendicular to the surface, thus can only exhibit BURGER's vectors without in-plane components which results in no possible edge dislocations. Furthermore, in this case, the BURGER's vectors of the two remaining r-planes have opposite tilt components, i.e. they point outwards and inwards of the surface, respectively. Regarding Equ. (1.16), this will result in no net tilt of the thin film.

Chapter 3

Experiment, Results and Discussion

Contents

Bibliography

[1] David S. Ginley, ed. *Handbook of Transparent Conductors*. Boston, MA: Springer US, 2011. ISBN: 978-1-4419-1637-2 978-1-4419-1638-9. DOI: 10.1007/978-1-4419-1638-9.

[2] C. Guillén and J. Herrero. "TCO/metal/TCO structures for energy and flexible electronics". In: *Thin Solid Films* 520.1 (2011), pp. 1–17. ISSN: 00406090. DOI: 10.1016/j.tsf.2011.06.091.

[3] Harpreet Singh and Bharpur Singh. "A brief study of novel transparent conducting oxide (TCO) material". In: 14th international conference on materials processing and characterization 2023. Hyderabad, India, 2024, p. 030164. DOI: 10.1063/5.0197252.

[4] Ganesh T. Chavan *et al.* "A Brief Review of Transparent Conducting Oxides (TCO): The Influence of Different Deposition Techniques on the Efficiency of Solar Cells". In: *Nanomaterials* 13.7 (2023), p. 1226. ISSN: 2079-4991. DOI: 10.3390/nano13071226.

[5] Chiara Candelise, Jamie F. Speirs, and Robert J.K. Gross. "Materials availability for thin film (TF) PV technologies development: A real concern?" In: *Renewable and Sustainable Energy Reviews* 15.9 (2011), pp. 4972–4981. ISSN: 13640321. DOI: 10.1016/j.rser.2011.06.012.

[6] Oleksiy Slobodyan *et al.* "Analysis of the dependence of critical electric field on semiconductor bandgap". In: *Journal of Materials Research* 37.4 (2022), pp. 849–865. ISSN: 0884-2914, 2044-5326. DOI: 10.1557/s43578-021-00465-2.

[7] Man Hoi Wong *et al.* "Ultrawide-bandgap semiconductors: An overview". In: *Journal of Materials Research* 36.23 (2021), pp. 4601–4615. ISSN: 0884-2914, 2044-5326. DOI: 10.1557/s43578-021-00458-1.

[8] Anna Hassa, Marius Grundmann, and Holger Von Wenckstern. "Progression of group-III sesquioxides: epitaxy, solubility and desorption". In: *Journal of Physics D: Applied Physics* 54.22 (2021), p. 223001. ISSN: 0022-3727, 1361-6463. DOI: 10.1088/1361-6463/abd4a4.

[9] S.I. Stepanov *et al.* "HVPE growth of corundum-structured α-Ga2O3 on sapphire substrates with α-Cr2O3 buffer layer". In: *Materials Physics and Mechanics* 47 (2021), pp. 577–581. DOI: 10.18149/MPM.4742021_4.

[10] Kentaro Kaneko, Taichi Nomura, and Shizuo Fujita. "Corundum-structured α-phase Ga_2O_3-Cr_2O_3-Fe_2O_3 alloy system for novel functions". In: *Phys. Status Solidi C* 7.10 (2010), pp. 2467–2470. ISSN: 1610-1642. DOI: 10.1002/pssc.200983896.

[11] N. Uekawa and K. Kaneko. "Dopant Reduction in *p*-Type Oxide Films upon Oxygen Absorption". In: *The Journal of Physical Chemistry* 100.10 (1996), pp. 4193–4198. ISSN: 0022-3654, 1541-5740. DOI: 10.1021/jp952784m.

[12] P. S. Robbert *et al.* "Novel electronic and magnetic properties of ultrathin chromium oxide films grown on Pt(111)". In: *Journal of Vacuum Science & Technology A: Vacuum, Surfaces, and Films* 16.3 (1998), pp. 990–995. ISSN: 0734-2101, 1520-8559. DOI: 10.1116/1.581283.

[13] M.F. Al-Kuhaili and S.M.A. Durrani. "Optical properties of chromium oxide thin films deposited by electron-beam evaporation". In: *Optical Materials* 29.6 (2007), pp. 709–713. ISSN: 09253467. DOI: 10.1016/j.optmat.2005.11.020.

[14] François Lebreau *et al.* "Structural, Magnetic, Electronic, Defect, and Diffusion Properties of Cr_2O_3: A DFT+U Study". In: *The Journal of Physical Chemistry C* 118.31 (2014), pp. 18133–18145. ISSN: 1932-7447. DOI: 10.1021/jp5039943.

[15] Zhishan Mi *et al.* "The effects of strain and vacancy defects on the electronic structure of Cr_2O_3". In: *Computational Materials Science* 144 (2018), pp. 64–69. ISSN: 09270256. DOI: 10.1016/j.commatsci.2017.12.012.

[16] R. W. G. Wyckoff. *Crystal structures*. New York, London, Sydney: Interscience Publishers, 1963. 467 pp.

[17] James F. Shackelford and William Alexander, eds. *Crc materials science and engineering handbook*. 0th ed. CRC Press, 2000. URL: https://doi.org/10.1201/9781420038408.

[18] F. D. Lai *et al.* "Ultrathin TiO_2 amorphous films for high transmittance APSM blanks at 157 and 193 nm wavelength simultaneously". In: *Journal of Vacuum Science & Technology B: Microelectronics and Nanometer Structures Processing, Measurement, and Phenomena* 21.6 (2003), pp. 3062–3066. ISSN: 1071-1023, 1520-8567. DOI: 10.1116/1.1624252.

[19] Jun C. Nable, Steven L. Suib, and Francis S. Galasso. "Metal organic chemical vapor deposition of Al_2O_3 and Cr_2O_3 on nickel as oxidation barriers". In: *Surface and Coatings Technology* 186.3 (2004), pp. 423–430. ISSN: 02578972. DOI: 10.1016/j.surfcoat.2003.11.022.

[20] Chun-Shen Cheng, H. Gomi, and H. Sakata. "Electrical and Optical Properties of Cr_2O_3 Films Prepared by Chemical Vapour Deposition". In: *Physica Status Solidi (a)* 155.2 (1996), pp. 417–425. ISSN: 00318965, 1521396X. DOI: 10.1002/pssa.2211550215.

[21] Cecilia Guillén and José Herrero. "Structural Changes Induced by Heating in Sputtered NiO and Cr_2O_3 Thin Films as *p*-Type Transparent Conductive Electrodes". In: *Electronic Materials* 2.2 (2021), pp. 49–59. ISSN: 2673-3978. DOI: 10.3390/electronicmat2020005.

[22] M. Catti *et al.* "Electronic, magnetic and crystal structure of Cr_2O_3 by theoretical methods". In: *Journal of Physics and Chemistry of Solids* 57.11 (1996), pp. 1735–1741. ISSN: 00223697. DOI: 10.1016/0022-3697(96)00034-0.

[23] Aoife B Kehoe *et al.* "Assessing the potential of Mg-doped Cr_2O_3 as a novel *p*-type transparent conducting oxide". In: *Journal of Physics: Condensed Matter* 28.12 (2016), p. 125501. ISSN: 0953-8984, 1361-648X. DOI: 10.1088/0953-8984/28/12/125501.

[24] Larry W. Finger and Robert M. Hazen. "Crystal structure and isothermal compression of Fe_2O_3, Cr_2O_3, and V_2O_3 to 50 kbars". In: *Journal of Applied Physics* 51.10 (1980), pp. 5362–5367. ISSN: 0021-8979, 1089-7550. DOI: 10.1063/1.327451.

[25] Elisabetta Arca *et al.* "Effect of Chemical Precursors On the Optical and Electrical Properties of *p*-Type Transparent Conducting Cr_2O_3:(Mg,N)". In: *The Journal of Physical Chemistry C* 117.42 (2013), pp. 21901–21907. ISSN: 1932-7447. DOI: 10.1021/jp404230k.

[26] Valerian Pishchik, Leonid A. Lytvynov, and Elena R. Dobrovinskaya. *Sapphire: Material, Manufacturing, Applications*. Boston, MA: Springer US, 2009. ISBN: 978-0-387-85694-0 978-0-387-85695-7. DOI: 10.1007/978-0-387-85695-7.

[27] M. Marezio and J. P. Remeika. "Bond lengths in the α-Ga_2O_3 structure and the high-pressure phase of $Ga_{2-x}Fe_xO_3$". In: *The Journal of Chemical Physics* 46.5 (1967), pp. 1862–1865. ISSN: 0021-9606, 1089-7690. DOI: 10.1063/1.1840945.

[28] Ruihua Cheng, C.N. Borca, and P.A. Dowben. "Selective Area Chemical Vapor Deposition of Chromium Oxides". In: *MRS Proceedings* 614 (2000), F10.4.1. ISSN: 0272-9172, 1946-4274. DOI: 10.1557/PROC-614-F10.4.1.

[29] Ruihua Cheng *et al.* "Potential phase control of chromium oxide thin films prepared by laser-initiated organometallic chemical vapor deposition". In: *Applied Physics Letters* 78.4 (2001), pp. 521–523. ISSN: 0003-6951, 1077-3118. DOI: 10.1063/1.1343846.

[30] L. Farrell *et al.* "Conducting mechanism in the epitaxial *p*-type transparent conducting oxide Cr_2O_3:Mg". In: *Physical Review B* 91.12 (2015), p. 125202. ISSN: 1098-0121, 1550-235X. DOI: 10.1103/PhysRevB.91.125202.

[31] E. Arca, K. Fleischer, and I. V. Shvets. "Magnesium, nitrogen codoped Cr_2O_3: A *p*-type transparent conducting oxide". In: *Applied Physics Letters* 99.11 (2011), p. 111910. ISSN: 0003-6951. DOI: 10.1063/1.3638461.

[32] Alexander Polyakov *et al.* "Electrical properties of α-Ga2O3 films grown by halide vapor phase epitaxy on sapphire with α-Cr2O3 buffers". In: *Journal of Applied Physics* 131.21 (2022), p. 215701. ISSN: 0021-8979, 1089-7550. DOI: 10.1063/5.0090832.

[33] Alexander Polyakov *et al.* "Effects of sapphire substrate orientation on Sn-doped α-Ga_2O_3 grown by halide vapor phase epitaxy using α-Cr_2O_3 buffers". In: *Journal of Physics D: Applied Physics* 55.49 (2022), p. 495102. ISSN: 0022-3727, 1361-6463. DOI: 10.1088/1361-6463/ac962f.

[34] Anna Caricato *et al.* "Deposition of chromium oxide thin films with large thermoelectromotive force coefficient by reactive pulsed laser ablation". In: *Journal of Optoelectronics and Advanced Materials* 12 (2010), p. 427.

[35] Sandhyarani Punugupati, Jagdish Narayan, and Frank Hunte. "Room temperature ferromagnetism in epitaxial Cr_2O_3 thin films grown on r-sapphire". In: *Journal of Applied Physics* 117.19 (2015), p. 193907. ISSN: 0021-8979, 1089-7550. DOI: 10.1063/1.4921435.

[36] Jarnail Singh *et al.* "Structural, optical and electrical characterization of epitaxial Cr_2O_3 thin film deposited by PLD". In: *Materials Research Express* 6.10 (2019), p. 106406. ISSN: 2053-1591. DOI: 10.1088/2053-1591/ab3543.

[37] Elisabetta Arca *et al.* "Valence band modification of Cr_2O_3 by Ni-doping: creating a high figure of merit *p*-type TCO". In: *Journal of Materials Chemistry C* 5.47 (2017), pp. 12610–12618. ISSN: 2050-7534. DOI: 10.1039/C7TC03545D.

[38] M. Tabbal *et al.* "Pulsed laser deposition of nanostructured dichromium trioxide thin films". In: *Thin Solid Films* 515.4 (2006), pp. 1976–1984. ISSN: 00406090. DOI: 10.1016/j.tsf.2006.08.010.

[39] Ruihua Cheng *et al.* "Characterization of the native Cr_2O_3 oxide surface of CrO_2". In: *Applied Physics Letters* 79.19 (2001), pp. 3122–3124. ISSN: 0003-6951, 1077-3118. DOI: 10.1063/1.1416474.

[40] P. Kofstad and K. P. Lillerud. "On High Temperature Oxidation of Chromium: II . Properties of and the Oxidation Mechanism of Chromium". In: *Journal of The Electrochemical Society* 127.11 (1980), pp. 2410–2419. ISSN: 0013-4651, 1945-7111. DOI: 10.1149/1.2129481.

[41] W. C. Hagel. "Electrical Conductivity of Li-Substituted Cr_2O_3". In: *Journal of Applied Physics* 36.8 (1965), pp. 2586–2587. ISSN: 0021-8979, 1089-7550. DOI: 10.1063/1.1714536.

[42] G. M. Crosbie *et al.* "Electronically Conducting Doped Chromium Oxides". In: *Journal of the American Ceramic Society* 67.7 (1984), pp. 498–503. ISSN: 0002-7820, 1551-2916. DOI: 10.1111/j.1151-2916.1984.tb19642.x.

[43] A Holt and P Kofstad. "Electrical conductivity and defect structure of Cr_2O_3. II. Reduced temperatures (<∼1000 °C)". In: *Solid State Ionics* 69.2 (1994), pp. 137–143. ISSN: 01672738. DOI: 10.1016/0167-2738(94)90402-2.

[44] Robert Schewski *et al.* "Epitaxial stabilization of pseudomorphic α-Ga_2O_3 on sapphire (0001)". In: *Applied Physics Express* 8.1 (2015), p. 011101. ISSN: 1882-0778, 1882-0786. DOI: 10.7567/APEX.8.011101.

[45] Clemens Petersen *et al.* "PLD of α-Ga_2O_3 on m-plane Al_2O_3: Growth regime, growth process, and structural properties". In: *APL Materials* 11.6 (2023), p. 061122. ISSN: 2166-532X. DOI: 10.1063/5.0149797.

[46] Kentaro Kaneko *et al.* "Progress in α-Ga_2O_3 for practical device applications". In: *Japanese Journal of Applied Physics* 62 (SF 2023), SF0803. ISSN: 0021-4922, 1347-4065. DOI: 10.35848/1347-4065/acd125.

[47] S. J. Pearton *et al.* "A review of Ga_2O_3 materials, processing, and devices". In: *Applied Physics Reviews* 5.1 (2018), p. 011301. ISSN: 1931-9401. DOI: 10.1063/1.5006941.

[48] Duyoung Yang *et al.* "Epitaxial growth of alpha gallium oxide thin films on sapphire substrates for electronic and optoelectronic devices: progress and perspective". In: *Electronic Materials Letters* 18.2 (2022), pp. 113–128. ISSN: 1738-8090, 2093-6788. DOI: 10.1007/s13391-021-00333-5.

[49] Kentaro Kaneko *et al.* "Evaluation of misfit relaxation in α-Ga_2O_3 epitaxial growth on α-Al_2O_3 substrate". In: *Japanese Journal of Applied Physics* 51 (2R 2012), p. 020201. ISSN: 0021-4922, 1347-4065. DOI: 10.1143/JJAP.51.020201.

[50] Sofie Vogt *et al.* "Realization of Conductive n-Type Doped α-Ga_2O_3 on *m*-Plane Sapphire Grown by a Two-Step Pulsed Laser Deposition Process". In: *physica status solidi (a)* 220.3 (2023), p. 2200721. ISSN: 1862-6300, 1862-6319. DOI: 10.1002/pssa.202200721.

[51] Riena Jinno *et al.* "Reduction in edge dislocation density in corundum-structured α-Ga_2O_3 layers on sapphire substrates with quasi-graded α-$(Al,Ga)_2O_3$ buffer layers". In: *Applied Physics Express* 9.7 (2016), p. 071101. ISSN: 1882-0778, 1882-0786. DOI: 10.7567/APEX.9.071101.

[52] Riena Jinno *et al.* "Crystal orientation dictated epitaxy of ultrawide-bandgap 5.4- to 8.6-eV α-$(AlGa)_2O_3$ on m-plane sapphire". In: *Science Advances* 7.2 (2021), eabd5891. ISSN: 2375-2548. DOI: 10.1126/sciadv.abd5891.

[53] Kazuaki Akaiwa *et al.* "Electrical properties of sn-doped α-ga_2o_3 films on *m*-plane sapphire substrates grown by mist chemical vapor deposition". In: *physica status solidi (a)* 217.3 (2020), p. 1900632. ISSN: 1862-6300, 1862-6319. DOI: 10.1002/pssa.201900632.

[54] Anna Hassa *et al.* "Control of phase formation of $(Al_xGa_{1-x})_2O_3$ thin films on c-plane Al_2O_3". In: *Journal of Physics D: Applied Physics* 53.48 (2020), p. 485105. ISSN: 0022-3727, 1361-6463. DOI: 10.1088/1361-6463/abaf7d.

[55] S. Vogt *et al.* "Zr doping in pulsed-laser-deposited α-Ga_2O_3 for device applications". In: *Physical Review Applied* 21.6 (2024), p. 064016. ISSN: 2331-7019. DOI: 10.1103/PhysRevApplied.21.064016.

[56] Neil W. Ashcroft and N. David Mermin. *Solid State Physics*. Saunders College Publishing, 1976. 826 pp.

[57] Marius Grundmann and Michael Lorenz. "Azimuthal anisotropy of rhombohedral (corundum phase) heterostructures". In: *physica status solidi (b)* 258.7 (2021), p. 2100104. ISSN: 1521-3951. DOI: 10.1002/pssb.202100104.

[58] George F. Harrington and José Santiso. "Back-to-Basics tutorial: X-ray diffraction of thin films". In: *Journal of Electroceramics* 47.4 (2021), pp. 141–163. ISSN: 1385-3449, 1573-8663. DOI: 10.1007/s10832-021-00263-6.

[59] Lothar Spieß, ed. *Moderne Röntgenbeugung: Röntgendiffraktometrie für Materialwissenschaftler, Physiker und Chemiker*. 2., überarb. und erw. Aufl. Studium. Wiesbaden: Vieweg + Teubner, 2009. 564 pp. ISBN: 978-3-8351-0166-1.

[60] L. D. Landau and E. M. Lifshitz. *Theory of Elasticity*. Course of Theoretical Physics vol. 7. Pergamon Press Ltd., 1970. 165 pp. ISBN: 978-0-08-057069-3.

[61] Marius Grundmann. "Elastic theory of pseudomorphic monoclinic and rhombohedral heterostructures". In: *Journal of Applied Physics* 124.18 (2018), p. 185302. ISSN: 0021-8979, 1089-7550. DOI: 10.1063/1.5045845.

[62] H.L. Alberts and J.C.A. Boeyens. "The elastic constants and distance dependence of the magnetic interactions of Cr_2O_3". In: *Journal of Magnetism and Magnetic Materials* 2.4 (1976), pp. 327–333. ISSN: 03048853. DOI: 10.1016/0304-8853(76)90044-5.

[63] Marius Grundmann. "A most general and facile recipe for the calculation of heteroepitaxial strain". In: *physica status solidi (b)* 257.12 (2020), p. 2000323. ISSN: 0370-1972, 1521-3951. DOI: 10.1002/pssb.202000323.

[64] Max Kneiß *et al.* "Strain states and relaxation for α-$(Al_xGa_{1-x})_2O_3$ thin films on prismatic planes of α-Al_2O_3 in the full composition range: Fundamental difference of a- and m-epitaxial planes in the manifestation of shear strain and lattice tilt". In: *Journal of Materials Research* 36.23 (2021), pp. 4816–4831. ISSN: 0884-2914, 2044-5326. DOI: 10.1557/s43578-021-00375-3.

[65] Marius Grundmann. *The Physics of Semiconductors: An Introduction Including Nanophysics and Applications*. Graduate Texts in Physics. Cham: Springer International Publishing, 2016. ISBN: 978-3-319-23879-1 978-3-319-23880-7. URL: http://link.springer.com/10.1007/978-3-319-23880-7.

[66] Derek Hull and D. J. Bacon. *Introduction to Dislocations*. 5th ed. Elsevier Ltd., 2011. 268 pp. ISBN: 978-0-08-096673-1.

[67] M. Grundmann and M. Lorenz. "Anisotropic strain relaxation through prismatic and basal slip in α-$(Al, Ga)_2O_3$ on R-plane Al_2O_3". In: *APL Materials* 8.2 (2020), p. 021108. ISSN: 2166-532X. DOI: 10.1063/1.5144744.

[68] M. Grundmann, T. Stralka, and M. Lorenz. "Epitaxial growth and strain relaxation of corundum-phase $(Al,Ga)_2O_3$ thin films from pulsed laser deposition at 1000 °C on r-plane Al_2O_3". In: *Applied Physics Letters* 117.24 (2020), p. 242102. ISSN: 0003-6951, 1077-3118. DOI: 10.1063/5.0030675.

[69] Michael Lorenz. "Pulsed laser deposition". In: *Encyclopedia of Applied Physics*. Wiley, 2019. URL: http://dx.doi.org/10.1002/3527600434.eap810.

[70] Holger von Wenckstern *et al.* "A review of the segmented-target approach to combinatorial material synthesis by pulsed-laser deposition". In: *Phy. Status Solidi B* 257.7 (2020), p. 1900626. ISSN: 0370-1972, 1521-3951. DOI: 10.1002/pssb.201900626.

[71] V. Srikant, J. S. Speck, and D. R. Clarke. "Mosaic structure in epitaxial thin films having large lattice mismatch". In: *Journal of Applied Physics* 82.9 (1997), pp. 4286–4295. ISSN: 0021-8979, 1089-7550. DOI: 10.1063/1.366235.

[72] L. J. van der Pauw. "A method of measuring specific resistivity and Hall effect of discs of arbitrary shape". In: *Philips Research Reports* 13.1 (1958), pp. 1–9.

[73] Hiroyuki Fujiwara. *Spectroscopic Ellipsometry. Principles and Applications*. Tōkyō: John Wiley & Sons, Ltd, 2007. ISBN: 978-4-621-07253-0.

[74] J.C. Manifacier *et al.* "Optical and electrical properties of SnO2 thin films in relation to their stoichiometric deviation and their crystalline structure". In: *Thin Solid Films* 41.2 (1977), pp. 127–135. ISSN: 00406090. DOI: 10.1016/0040-6090(77)90395-9.

[75] A. R. Zanatta. "Revisiting the optical bandgap of semiconductors and the proposal of a unified methodology to its determination". In: *Scientific Reports* 9.1 (2019), p. 11225. ISSN: 2045-2322. DOI: 10.1038/s41598-019-47670-y.

[76] Jan Tauc. "Optical properties of amorphous semiconductors and solar cells". In: *Fundamentals of Semiconductors*. 3rd ed. Berlin, Heidelberg: Springer, 2005. ISBN: 3-540-41323-5.

[77] Alex Dolgonos, Thomas O. Mason, and Kenneth R. Poeppelmeier. "Direct optical band gap measurement in polycrystalline semiconductors: A critical look at the Tauc method". In: *Journal of Solid State Chemistry* 240 (2016), pp. 43–48. ISSN: 00224596. DOI: 10.1016/j.jssc.2016.05.010.

[78] Mohamed A. Hafez, Mohamed K. Zayed, and Hani E. Elsayed-Ali. "Review: Geometric interpretation of reflection and transmission RHEED patterns". In: *Micron* 159 (2022), p. 103286. ISSN: 09684328. DOI: 10.1016/j.micron.2022.103286.

[79] Anubhav Jain *et al.* "Commentary: The Materials Project: A materials genome approach to accelerating materials innovation". In: *APL Materials* 1.1 (2013), p. 011002. ISSN: 2166-532X. DOI: 10.1063/1.4812323.